

## Article

# Preparation of BiOCl/Bi<sub>2</sub>WO<sub>6</sub> Photocatalyst for Efficient Fixation on Cotton Fabric: Applications in UV Shielding and Self-Cleaning Performances

Jiayi Chen <sup>1</sup>, Kuang Wang <sup>1,2</sup>, Jialong Tian <sup>1</sup>, Wenhui Yu <sup>1,3</sup>, Yujie Chen <sup>1,3</sup>, Na Li <sup>1</sup>, Zhenming Qi <sup>1</sup> and Chunxia Wang <sup>1,3,\*</sup>

<sup>1</sup> College of Textile and Clothing, Yancheng Institute of Technology, Yancheng 224051, China; jychen1982@163.com (J.C.); wkmineking@163.com (K.W.); jialongtian1996@163.com (J.T.); Eleanor980119@163.com (W.Y.); 2012310002@stmail.ntu.edu.cn (Y.C.); linahww@163.com (N.L.); stoner28@126.com (Z.Q.)

<sup>2</sup> School of Textile Science and Engineering, Jiangnan University, Wuxi 214122, China

<sup>3</sup> School of Textile and Clothing, Nantong University, Nantong 226019, China

\* Correspondence: cxwang@mail.dhu.edu.cn; Tel.: +86-180-6889-1566

**Abstract:** In this work, a visible-light-driven BiOCl/Bi<sub>2</sub>WO<sub>6</sub> photocatalyst was obtained via a facile hydrothermal method and characterized by X-ray diffraction (XRD), scanning electron microscopy (SEM), energy-dispersive spectrometry (EDS), X-ray photoelectron spectroscopy (XPS), ultraviolet/visible light diffuse reflection spectroscopy (UV/Vis), and photocurrent (PC). BiOCl/Bi<sub>2</sub>WO<sub>6</sub> was modified with (3-chloro-2-hydroxypropyl) trimethyl ammonium chloride to obtain the cationized BiOCl/Bi<sub>2</sub>WO<sub>6</sub>. Cotton fabric was pretreated with sodium hydroxide (NaOH) and sodium chloroacetate solution to obtain carboxymethylated cotton fabric, which was further reacted with cationized BiOCl/Bi<sub>2</sub>WO<sub>6</sub> to achieve finished cotton fabric. The cotton fabrics were characterized by Fourier-transform infrared spectroscopy (FT-IR), XRD, SEM, and EDS. The photocatalytic activity of the BiOCl/Bi<sub>2</sub>WO<sub>6</sub> photocatalyst and cotton fabrics was assessed by photocatalytic degradation of MB (methylene blue) solution under simulated visible light. The self-cleaning property of cotton fabrics was evaluated by removing MB solution and red-wine stains. Results revealed that the coated cotton fabrics exhibited appreciable photocatalytic and self-cleaning performance. In addition, anti-UV studies showed that the finished cotton fabrics had remarkable UV blocking properties in the UVA and UVB regions. Therefore, the finished cotton fabric with BiOCl/Bi<sub>2</sub>WO<sub>6</sub> can provide a framework for the development of multifunctional textiles.

**Keywords:** BiOCl/Bi<sub>2</sub>WO<sub>6</sub>; cotton fabric; UV shielding; photocatalysis; self-cleaning



**Citation:** Chen, J.; Wang, K.; Tian, J.; Yu, W.; Chen, Y.; Li, N.; Qi, Z.; Wang, C. Preparation of BiOCl/Bi<sub>2</sub>WO<sub>6</sub> Photocatalyst for Efficient Fixation on Cotton Fabric: Applications in UV Shielding and Self-Cleaning Performances. *Materials* **2021**, *14*, 7002. <https://doi.org/10.3390/ma14227002>

Academic Editor: Juan M. Coronado

Received: 1 November 2021

Accepted: 15 November 2021

Published: 18 November 2021

**Publisher's Note:** MDPI stays neutral with regard to jurisdictional claims in published maps and institutional affiliations.



**Copyright:** © 2021 by the authors. Licensee MDPI, Basel, Switzerland. This article is an open access article distributed under the terms and conditions of the Creative Commons Attribution (CC BY) license (<https://creativecommons.org/licenses/by/4.0/>).

## 1. Introduction

Semiconductor-based photocatalysis is regarded as a promising and cost-effective approach to realize environmental decontamination [1–5]. Traditional semiconductor materials with a wide bandgap (e.g., TiO<sub>2</sub>, ZnO, and BiOCl) are widely utilized in practical application due to their commendable chemical stability, biosafety, photostability, and low cost [6–9]. BiOCl with a layered structure is a potential candidate for semiconductor photocatalysis owing to its superior photocatalytic activity. However, it displays a relatively low quantum efficiency in the visible wavelength range that hinders its practical implementation [8–11]. Another bismuth compound, namely, Bi<sub>2</sub>WO<sub>6</sub>, with its comparatively narrow bandgap, is capable of adsorbing visible light. Nevertheless, the rapid recombination of photogenerated electron–hole pairs in Bi<sub>2</sub>WO<sub>6</sub> reduces its photocatalytic efficiency [12–14]. Interestingly, the lattice of Bi<sub>2</sub>WO<sub>6</sub> and BiOCl can be well matched and form heterojunctions to promote the separation of photogenerated carriers [15,16]. Tahmasebi et al. fabricated a Bi<sub>2</sub>WO<sub>6</sub>/BiOCl composite through a facile hydrothermal method with the aid of hydrochloric acid (HCl) as a Cl source, and the obtained Bi<sub>2</sub>WO<sub>6</sub>/BiOCl

exhibited preferable photocatalytic activity [17]. Visible light-responsive  $\text{Bi}_2\text{WO}_6/\text{BiOCl}$  heterojunctions were successfully prepared via a simple one-step hydrothermal method by Liang and his coworkers, and the results revealed that  $\text{Bi}_2\text{WO}_6/\text{BiOCl}$  had superior degradation efficiency under visible-light illumination than bare  $\text{BiOCl}$  and  $\text{Bi}_2\text{WO}_6$  [18].

Cotton fabric is a very common natural fabric that has been widely used as the substrate of functional textiles due to its exceptional moisture absorption, breathability, comfortability, etc. [19–22]. Cotton fabrics have been finished with semiconductor materials by many researchers to obtain properties such as self-cleaning, UV-shielding, superhydrophobic, water–oil separating, and antibacterial [23–25]. Tudu et al. developed a superhydrophobic cotton fabric using a mixture of perfluorodecyltriethoxysilane (PFDTs) and  $\text{TiO}_2$  nanoparticles, and the coated cotton fabric presented outstanding self-cleaning, stain resistance, rust stain resistance, antiwater absorption, and antibacterial abilities [26].  $\text{BiOCl}$  nanosheet-coated cotton fabric was obtained via a pad–dry–cure method by Jin and his colleagues; the finished cotton fabric showed appreciable UV protection and photocatalytic performance [27]. To the best of our knowledge, a cotton fabric finished with  $\text{BiOCl}/\text{Bi}_2\text{WO}_6$  photocatalyst has not been reported to study its various functionalities, such as self-cleaning, UV-shielding, and photocatalytic properties.

In this study, we coupled  $\text{BiOCl}$  with  $\text{Bi}_2\text{WO}_6$  through a facile one-step hydrothermal method and characterized it by XRD, SEM, EDS, XPS, UV/Vis DRS, PC, and photocatalytic activity. Thereafter, the cotton fabric was pretreated by  $\text{NaOH}$  and sodium chloroacetate solution to obtain carboxymethylated cotton fabric, and then finished with cationized  $\text{BiOCl}/\text{Bi}_2\text{WO}_6$  to obtain multifunctional cotton fabric via double-dip/double-roll technology. The UV protection, photocatalytic, and self-cleaning properties of the cotton fabric coated with  $\text{BiOCl}/\text{Bi}_2\text{WO}_6$  were investigated.

## 2. Experimental

### 2.1. Materials

Bismuth nitrate pentahydrate ( $\text{Bi}(\text{NO}_3)_3 \cdot 5\text{H}_2\text{O}$ , AR) and methylene blue (MB, AR) were purchased from Tianjin Damao Chemical Reagent Co., Ltd. (Tianjin, China). Sodium tungstate dehydrate ( $\text{Na}_2\text{WO}_4 \cdot 2\text{H}_2\text{O}$ , AR), acetic acid ( $\text{CH}_3\text{COOH}$ , AR), and anhydrous ethanol (AR) were obtained from Sinopharm Chemical Reagent Co., Ltd. Sodium chloride ( $\text{NaCl}$ , AR) and sodium hydroxide ( $\text{NaOH}$ , AR) were provided by Jiangsu Tongsheng Chemical Reagent Co., Ltd. (Yixing, China). (3-Chloro-2-hydroxypropyl) trimethyl ammonium chloride (60%, AR) and sodium chloroacetate (AR) were purchased from Aladdin Biochemical Technology Co., Ltd. (Shanghai, China). Red wine (food grade) was bought from Greatwall Wine (Beijing, China). Cotton fabric (linear density, 20 tex  $\times$  20 tex; fabric density, 300 fiber/10 cm  $\times$  300 fiber/10 cm; weight,  $(120 \pm 10)$  g/m<sup>2</sup>; plain) was obtained from Nantong Weiteng Textile Co., Ltd. (Nantong, China).

### 2.2. Preparation of $\text{BiOCl}/\text{Bi}_2\text{WO}_6$

In a typical preparation run [28], 5 mmol of  $\text{Bi}(\text{NO}_3)_3 \cdot 5\text{H}_2\text{O}$  was added to 40 mL of deionized water under ultrasonic oscillation for 30 min. An appropriate amount of  $\text{NaCl}$  was added to the aforementioned suspension and stirred for 30 min. Simultaneously, a stoichiometric amount of  $\text{Na}_2\text{WO}_4 \cdot 2\text{H}_2\text{O}$  was dissolved in 20 mL of deionized water to obtain a uniformly transparent solution and was added dropwise to the above mixture under constant magnetic stirring (Shanghai Sile Instruments Co. Ltd., Shanghai, China) for 60 min. The mixture was transferred to a 100 mL Teflon-lined stainless-steel autoclave and maintained at 160 °C for 8 h. After the reaction, the precipitate was centrifuged and rinsed with deionized water and anhydrous ethanol three times. Finally, the samples were dried at 60 °C for 10 h to acquire  $\text{BiOCl}/\text{Bi}_2\text{WO}_6$ . The prepared samples with Cl and W at molar ratios of 1:3, 1:2, 1:1, 2:1, and 3:1 were denoted Cl/W-1-3, Cl/W-1-2, Cl/W-1-1, Cl/W-2-1, and Cl/W-3-1, respectively. For comparison, bare  $\text{Bi}_2\text{WO}_6$  and  $\text{BiOCl}$  were prepared without adding  $\text{NaCl}$  and  $\text{Na}_2\text{WO}_4 \cdot 2\text{H}_2\text{O}$  under the same conditions.

### 2.3. Modification of $\text{BiOCl}/\text{Bi}_2\text{WO}_6$

In brief, 5 g of (3-chloro-2-hydroxypropyl) trimethyl ammonium chloride was dissolved in 100 mL of deionized water under sonication for 30 min. The solution was added with 1 g of  $\text{BiOCl}/\text{Bi}_2\text{WO}_6$  (Cl/W-1-2) and stirred for 30 min. The precipitate was collected by centrifugation (Changsha Xiangyi Centrifuge Instrument Co. Ltd., Changsha, China) and dried in an oven (Shanghai Jing Hong Laboratory instruments Co. Ltd., Shanghai, China) at 60 °C for 12 h to obtain modified  $\text{BiOCl}/\text{Bi}_2\text{WO}_6$  powder [29].

### 2.4. Pretreatment of Cotton Fabrics

**Alkalized cotton fabrics:** Cotton fabrics were cut into 6 cm × 6 cm pieces and washed in an ultrasound water bath to remove impurities. The pieces were immersed in NaOH aqueous solution (15 wt.%) at 20 °C for 10 min, rinsed with deionized water, and dried at 60 °C to obtain alkalized cotton fabrics.

**Carboxymethylated cotton fabrics:** In brief, 10 g of sodium chloroacetate was dissolved in 100 mL of ethanol/water ( $v/v = 6/4$ ) solution. The prepared alkalized cotton fabrics were immersed in the above solution at 20 °C for 10 min and then dried at 70 °C for 1 h. The cotton substrates were washed by deionized water, treated with 2 g/L acetic acid solution, washed with deionized water, and dried at 60 °C to obtain carboxymethylated cotton fabrics [30].

### 2.5. Finishing of Cotton Fabrics

First, 0.1 g, 0.2 g, and 0.3 g of modified  $\text{BiOCl}/\text{Bi}_2\text{WO}_6$  were dispersed in 50 mL of deionized water under ultrasonication (Kunshan Ultrasonic Instrument Co. Ltd., Suzhou, China) for 30 min to form a uniform suspension. From the schematic diagram of the preparation of  $\text{BiOCl}/\text{Bi}_2\text{WO}_6$ -cotton fabrics as shown in Figure 1, 1 g of the carboxymethylated cotton fabrics were soaked in the above suspension for 30 min. The cotton fabrics were finished via the double-dip/double-roll technology and dried at 60 °C to achieve cotton fabrics functionalized with  $\text{BiOCl}/\text{Bi}_2\text{WO}_6$ . The cotton fabrics were labeled Cl/W-0.1 cotton fabric, Cl/W-0.2 cotton fabric, and Cl/W-0.3 cotton fabric on the basis of the amount of modified  $\text{BiOCl}/\text{Bi}_2\text{WO}_6$ .

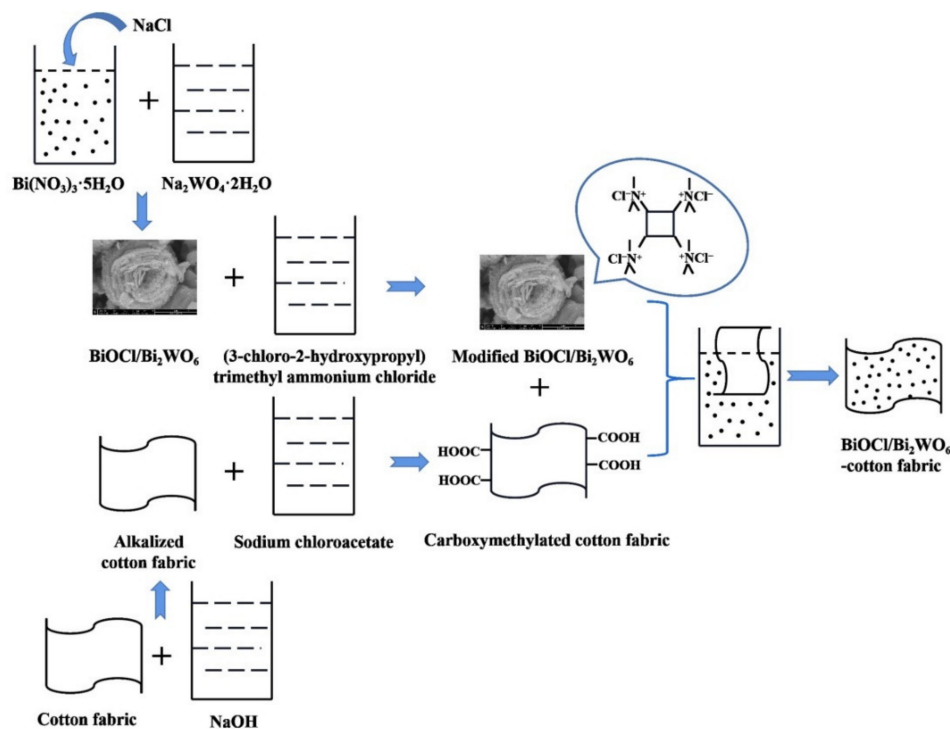


**Figure 1.** Schematic diagram of the preparation of  $\text{BiOCl}/\text{Bi}_2\text{WO}_6$ -cotton fabrics.

## 2.6. Characterization

X-ray diffraction was investigated using an X PERT3 POWDER diffractometer (PANalytical, Amsterdam, The Netherlands) to detect the crystalline structures of the as-prepared samples. Surface morphologies were characterized using a Nova Nano SEM 450 field-emission scanning electron microscope (FEI, Hillsboro, OR, USA). The SEM was equipped with a VANTAGE-DS1 energy-dispersive spectrometer (Oxford Instruments, Oxford, UK) to study the elemental compositions and their contents. X-ray photoelectron spectra were recorded on an ESCALAB 250Xi X-ray photoelectron spectrometer (Thermo Fisher Scientific, Waltham, MA, USA) to investigate the surface chemical states and their composite structures. UV/Vis diffuse reflectance spectra were inspected using TU-1901 UV/Vis diffuse reflectometer (Persee, Beijing, China) with the wavelength of 200–800 nm to record the optical absorption properties. Fourier-transform infrared spectra were recorded using a NEXUF-670 Fourier infrared spectrometer (NICOLET, Madison, GA, USA) to evaluate the chemical compositions. Photoelectric properties were measured on a CHI 660D electrochemical workstation (CHI, Shanghai, China) with a three-electrode system.

## 2.7. Photocatalytic Activity Measurement

Photocatalytic activities of photocatalyst and cotton fabric were determined via the photodegradation of aqueous MB and RhB (Rhodamine B) under simulated visible-light illumination. Typically, 0.01 g of the as-obtained photocatalyst was dispersed in 100 mL of 10 mg/L aqueous MB to form a suspension. Cotton samples (6 cm × 6 cm) were cut into 1 cm × 1 cm pieces and placed in 50 mL of 10 mg/L RhB solution under magnetic stirring (Shanghai Sile Instruments Co. Ltd., Shanghai, China). After being agitated in the dark for 30 min to reach the adsorption–desorption equilibrium, the suspension was irradiated and constantly stirred under a 300 W xenon lamp (Perfect Light, Beijing, China) with a 400 nm cut-off filter. About 3 mL of the reaction solution was taken at the 10 min time interval and then centrifuged for 5 min to remove photocatalyst particles. The absorbances of aqueous MB and RhB were investigated by UV/Vis spectrophotometry at 664 nm and 554 nm with deionized water as the reference at time intervals of 10 min during photocatalytic reaction. The photodegradation rate was calculated as the ratio of the concentration difference before and after irradiation compared with the concentration before irradiation (Equation (1)).

$$D = (1 - C_t/C) \times 100\%, \quad (1)$$

where  $D$  is the photodegradation rate,  $C$  is the absorbance of 10 mg/L aqueous MB and RhB, and  $C_t$  is the absorbance of aqueous MB and RhB after  $t$  min of illumination [31,32].

## 2.8. Assessment of Cotton Fabrics

UV-blocking performance of cotton fabrics was recorded by YG (B) 912E textile anti-UV performance tester (Darong, Wenzhou, China).

Self-cleaning performance was assessed with aqueous MB and red wine as the stains. In brief, 0.2 mL of 20 mg/L MB and red wine were dropped on the cotton fabrics (6 cm × 6 cm). After drying in air under ambient conditions, the samples were irradiated by simulated visible light [26]. The photos were taken at intervals of 40 min.

## 3. Results and Discussion

### 3.1. XRD Analysis of the Photocatalysts

XRD analysis is performed to investigate the crystal structure of the sample, and the powder XRD pattern is shown in Figure 2. The peaks at 11.98°, 24.09°, 25.86°, 32.49°, and 33.45° were assigned to the (001), (002), (101), (110), and (102) planes of tetragonal phase BiOCl (JCPDS No. 06-0249) [33,34]. The sharp and narrow peaks indicate the distinctive monophase of the good crystallinity of BiOCl. The diffraction peaks at  $2\theta = 28.31^\circ$ ,  $32.79^\circ$ ,  $47.16^\circ$ , and  $55.83^\circ$  were attributed to the (113), (200), (220), and (313) planes of orthorhombic russelite phase Bi<sub>2</sub>WO<sub>6</sub> (JCPDS No. 73-1126), and no other impurity

peaks were identified [35]. BiOCl/Bi<sub>2</sub>WO<sub>6</sub> in Figure 2b–e exhibited a consistent position in the XRD patterns, indicating that all the samples were BiOCl/Bi<sub>2</sub>WO<sub>6</sub>. Moreover, no diffraction peaks of BiOCl were detected in Cl/W-1-3 from Figure 2a, which may be due to the insufficient content of BiOCl/Bi<sub>2</sub>WO<sub>6</sub>.

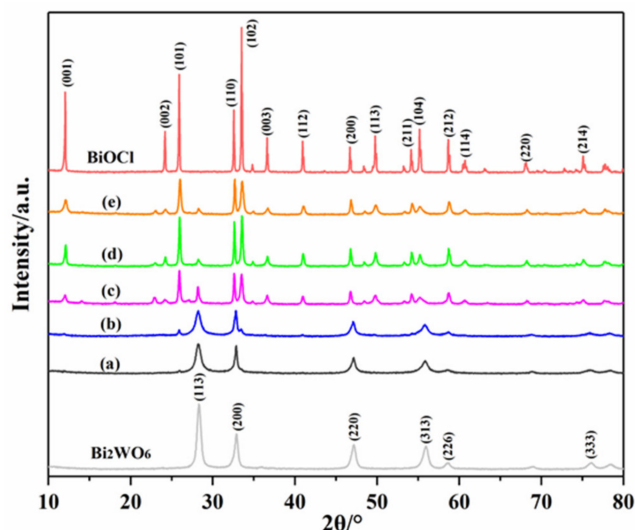


**Figure 2.** XRD patterns: Bi<sub>2</sub>WO<sub>6</sub>, (a) Cl/W-1-3, (b) Cl/W-1-2, (c) Cl/W-1-1, (d) Cl/W-2-1, (e) Cl/W-3-1, and BiOCl.

### 3.2. SEM and EDS Analyses of the Photocatalysts

Figure 3 displays the SEM images and EDS of Cl/W-1-2. As displayed in Figure 3a,b, nanoflower-shaped Cl/W-1-2, 2–3  $\mu\text{m}$  in diameter, was composed of hierarchical nanosheets. EDS is illustrated in Figure 3c to further reveal the chemical components of Cl/W-1-2. The weight percentages of Bi, W, O, and Cl accounted for 72.78%, 6.93%, 10.17%, and 10.13%, respectively, which verified the successful fabrication of BiOCl/Bi<sub>2</sub>WO<sub>6</sub>.

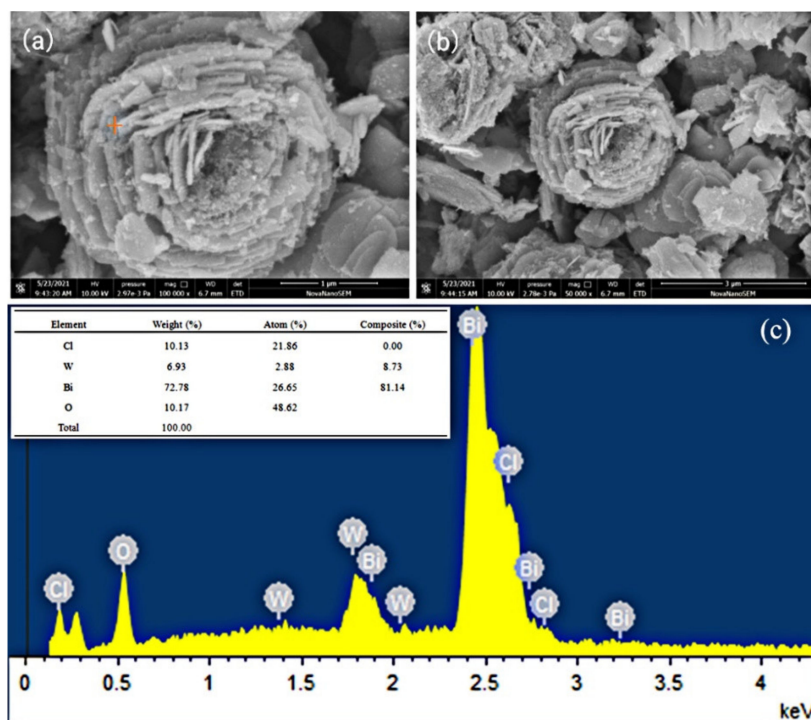


**Figure 3.** SEM images and EDS of Cl/W-1-2: (a) Cl/W-1-2 ( $\times 100,000$ ), (b) Cl/W-1-2 ( $\times 50,000$ ), and (c) EDS of Cl/W-1-2.

### 3.3. XPS Analysis

Figure 4 presents the XPS spectra of Cl/W-1-2. The XPS survey spectrum in Figure 4a revealed that the Cl/W-1-2 composite contains Bi, O, Cl, and W, while C was the residue of the apparatus. The contents of Bi, O, Cl, and W accounted for about 59.75%, 15.29%, 4.22%, and 20.73%, respectively. The peaks at 159.5 eV and 164.7 eV in Figure 4b corresponded to Bi 4f<sub>7/2</sub> and Bi 4f<sub>5/2</sub>, respectively, which confirmed the presence of Bi<sup>3+</sup> ions [36]. The peaks at 530.0 eV and 531.8 eV in Figure 4c could be ascribed to the lattice oxygen of the BiOCl/Bi<sub>2</sub>WO<sub>6</sub> composite and the hydroxyl groups of the absorbed H<sub>2</sub>O molecules, respectively [37]. The Cl 2p spectrum in Figure 4d was fitted by two peaks with the binding energy at 199.8 eV and 198.2 eV, corresponding to Cl 2p<sub>1/2</sub> and Cl 2p<sub>3/2</sub> peaks, respectively [38]. The two peaks at 36 eV and 38.1 eV in Figure 4e were in accordance with W 4f<sub>7/2</sub> and W 4f<sub>5/2</sub>, respectively, corresponding to W<sup>6+</sup> in BiOCl/Bi<sub>2</sub>WO<sub>6</sub> [39]. The XPS analysis proved that BiOCl was successfully coupled with Bi<sub>2</sub>WO<sub>6</sub>, which was consistent with the XRD patterns.

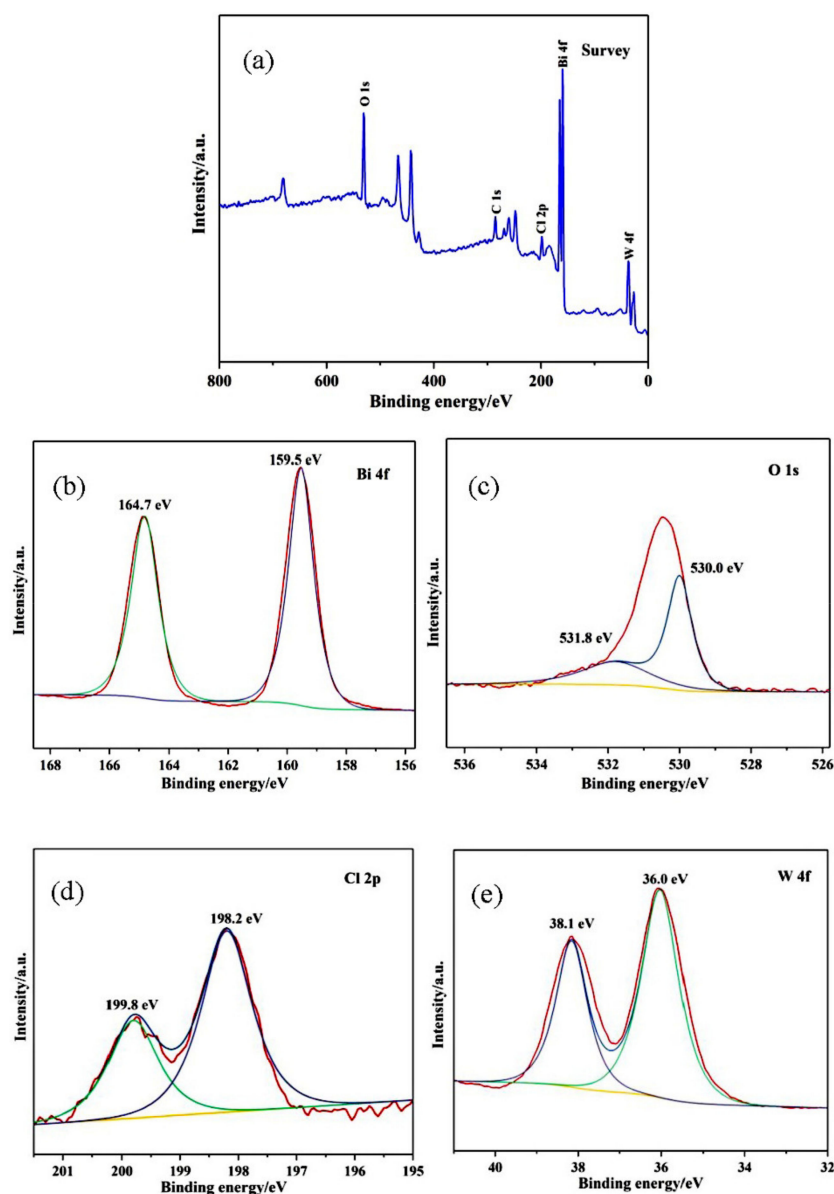


Figure 4. XPS spectra of Cl/W-1-2: (a) survey, (b) Bi 4f, (c) O 1s, (d) Cl 2p, and (e) W 4f.

### 3.4. UV/Vis DRS Analysis of the Photocatalysts

UV/Vis DRS of  $\text{Bi}_2\text{WO}_6$ , Cl/W-1-2, and BiOCl are given in Figure 5. The absorption bandgap energy of the as-prepared samples was estimated according to  $E_g = 1240/\lambda_g$ , where  $E_g$  is the bandgap and  $\lambda_g$  is the absorption edge [40]. As shown in Figure 5, the absorption edges of  $\text{Bi}_2\text{WO}_6$ , Cl/W-1-2, and BiOCl at about 444 nm, 415 nm, and 375 nm were inspected. The bandgaps of  $\text{Bi}_2\text{WO}_6$ , Cl/W-1-2 and BiOCl were calculated to be 2.79 eV, 2.98 eV, and 3.31 eV, respectively. Compared with BiOCl, Cl/W-1-2 exhibited a relatively narrower bandgap and, therefore, an expanded photoreponse range.

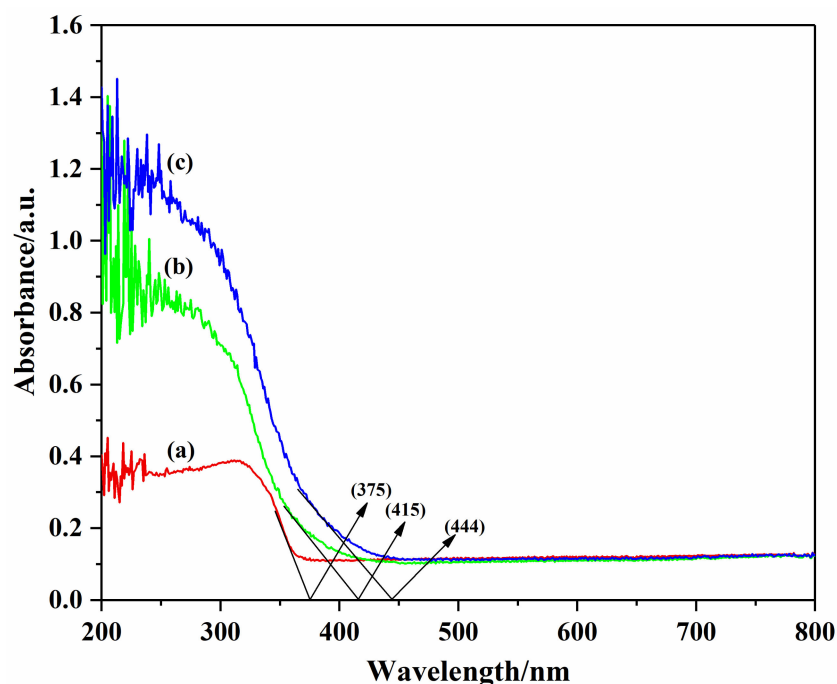


Figure 5. UV/Vis DRS of the photocatalysts: (a) BiOCl, (b) Cl/W-1-2, and (c)  $\text{Bi}_2\text{WO}_6$ .

### 3.5. PC Analysis of the Photocatalysts

The photoelectrochemical properties of the photocatalysts were investigated to determine the photocatalytic activity under simulated visible light. PC intensity is an index of recombination efficiency of photogenerated electron–hole pairs. A higher PC intensity denotes a lower recombination of photogenerated carriers. As shown in Figure 6, the PC intensity of Cl/W-1-2 was higher than that of  $\text{Bi}_2\text{WO}_6$  and BiOCl. This might be explained by the increasing interfacial charge carrier transfer efficiency and the decreasing photogenerated carrier recombination, owing to the combination of  $\text{Bi}_2\text{WO}_6$  and BiOCl. The result showed that Cl/W-1-2 was beneficial to the photocatalytic degradation of pollutants.

### 3.6. Photocatalytic Activity of the Photocatalysts

Figure 7 displays the photocatalytic activities and pseudo-first-order kinetic models of the as-prepared samples under simulated visible-light irradiation. As shown in Figure 7a, BiOCl showed poor photocatalytic efficiency, while the other photocatalysts exhibited definite adsorption of MB solution in the dark reaction. The photodegradation rate for BiOCl/ $\text{Bi}_2\text{WO}_6$  increased with the increasing content of W. The photocatalyst had no obvious change when the molar ratio of Cl to W reached 1:2. Furthermore, Cl/W-3-1 showed a higher degradation rate than BiOCl but a lower one than  $\text{Bi}_2\text{WO}_6$ , which may be attributed to the insufficient content of W. The heterostructure of BiOCl/ $\text{Bi}_2\text{WO}_6$  restrained the recombination of electron–hole pairs to increase the surface active sites, thereby enhancing the photocatalytic capacity. Cl/W-1-2 had good photodegradation of MB as high as 90% in 60 min. Hence, Cl/W-1-2 ranked the first in the photodegradation of MB under visible-light irradiation.

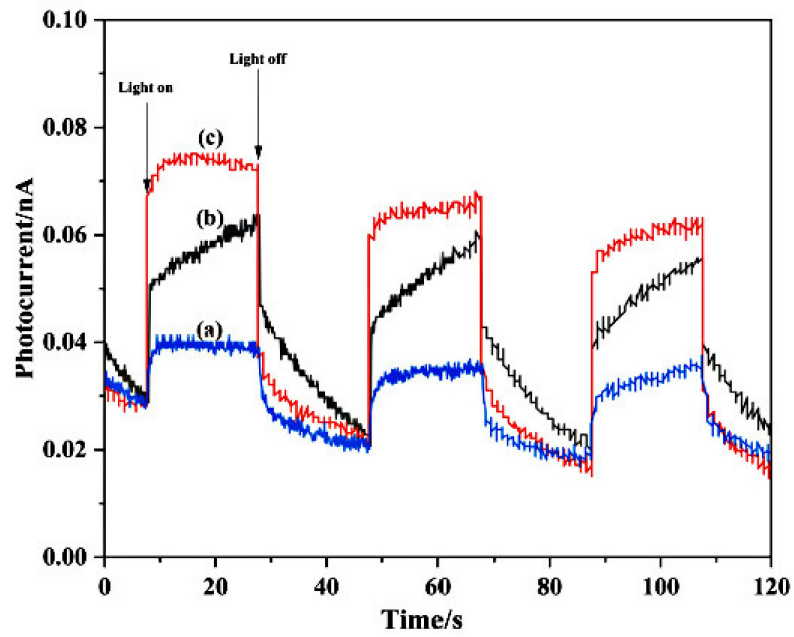


Figure 6. Photocurrent of the photocatalysts: (a) BiOCl, (b) Bi<sub>2</sub>WO<sub>6</sub>, and (c) Cl/W-1-2.

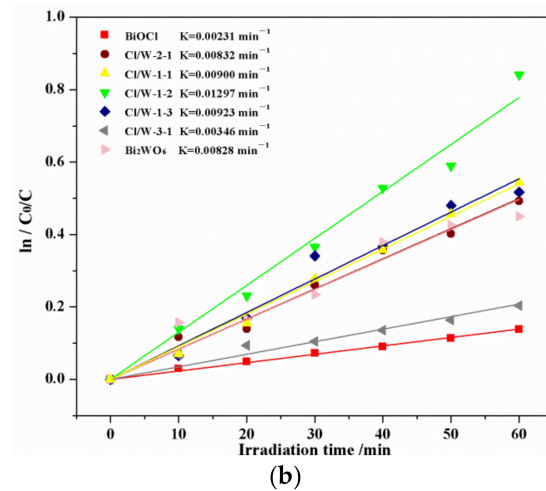
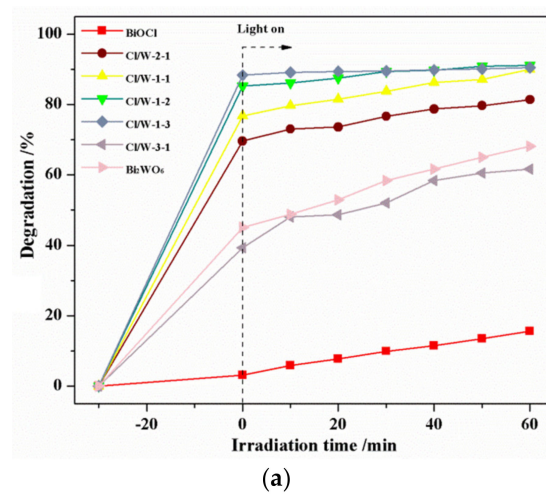


Figure 7. Photocatalytic degradation for MB by photocatalysts: (a) photodegradation curves and (b) pseudo-first-order kinetic curves.

### 3.7. XRD Analysis of Cotton Fabrics

Figure 8 presents the XRD patterns of cotton fabric, Cl/W-0.3 cotton fabric, and Cl/W-1-2. As shown in Figure 8a, the diffraction peaks at  $2\theta$  of  $14.9^\circ$ ,  $16.6^\circ$ ,  $22.6^\circ$ , and  $34.4^\circ$  were observed in cotton fabric, corresponding to the (101), (110), (002), and (040) planes of cellulose [41,42]. As shown in Figure 8c, the diffraction peaks at  $2\theta = 28.3^\circ$ ,  $36.7^\circ$ ,  $47.1^\circ$ , and  $53.5^\circ$  were indexed to the (113), (016), (220), and (131) planes of  $\text{Bi}_2\text{WO}_6$  (JCPDS No. 73-1126), while the diffraction peaks at  $2\theta$  of  $11.9^\circ$ ,  $25.8^\circ$ ,  $32.5^\circ$ ,  $58.6^\circ$ , and  $74.9^\circ$  were related to the (001), (101), (110), (212), and (214) planes of  $\text{BiOCl}$  (JCPDS NO. 06-0249). In the XRD pattern of Cl/W-0.3 cotton fabric in Figure 8b, the (101), (110), (002), and (040) planes of the cellulose, as well as the (001), (101), (110), (212), and (220) planes of the modified  $\text{BiOCl}/\text{Bi}_2\text{WO}_6$  photocatalyst, were observed. According to the above analysis, the modified  $\text{BiOCl}/\text{Bi}_2\text{WO}_6$  was successfully loaded onto cotton fabric.

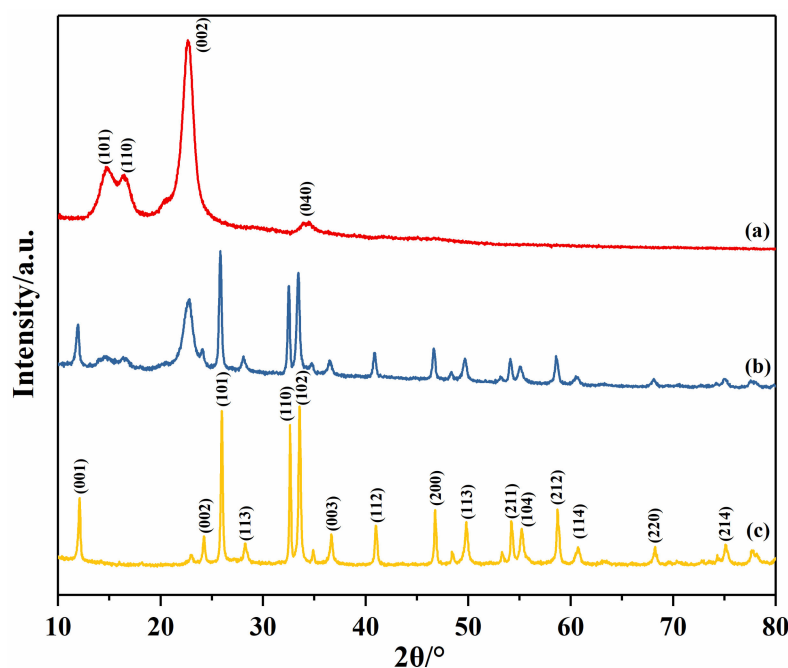


Figure 8. XRD patterns: (a) cotton fabric, (b) Cl/W-0.3 cotton fabric, and (c) Cl/W-1-2.

### 3.8. FT-IR Analysis

The typical FT-IR spectra of cotton fabric, Cl/W-1-2, and Cl/W-0.3 measured within  $400\text{--}4000\text{ cm}^{-1}$  are illustrated in Figure 9. For the cotton fabric in Figure 9a, the absorption peaks at  $3440\text{ cm}^{-1}$  and  $2910\text{ cm}^{-1}$  were respectively derived from the stretching vibrations of  $-\text{OH}$  groups and  $-\text{CH}/\text{CH}_2$  groups in cotton fabric. The absorption peak at  $1636\text{ cm}^{-1}$  was credited to the absorption peak of water molecules on the cotton surface. The absorption peaks at  $1110\text{ cm}^{-1}$  and  $1156\text{ cm}^{-1}$  were related to the symmetrical and asymmetrical stretching vibrations of  $\text{C}-\text{O}-\text{C}$  in cotton fabric. Cl/W-1-2 in Figure 9b also contained  $-\text{OH}$  groups, whose absorption peak of stretching vibration corresponded to  $3440\text{ cm}^{-1}$ . The peak at  $1607\text{ cm}^{-1}$  was generated by the absorption peak of water molecules. The  $\text{Bi}-\text{O}$  absorption peak and  $\text{W}-\text{O}$  asymmetrical stretching vibration peak appeared at  $400\text{--}636\text{ cm}^{-1}$ . After loading with modified  $\text{BiOCl}/\text{Bi}_2\text{WO}_6$ , Cl/W-0.3 cotton fabric in Figure 9c presented a similar shape and position of absorption peaks as cotton fabric between  $1093$  and  $4000\text{ cm}^{-1}$ . Furthermore, the absorption bands at  $400\text{--}639\text{ cm}^{-1}$  were assigned to Cl/W-1-2. The results showed that the  $\text{BiOCl}/\text{Bi}_2\text{WO}_6$  photocatalyst was successfully loaded on cotton fabric [34].

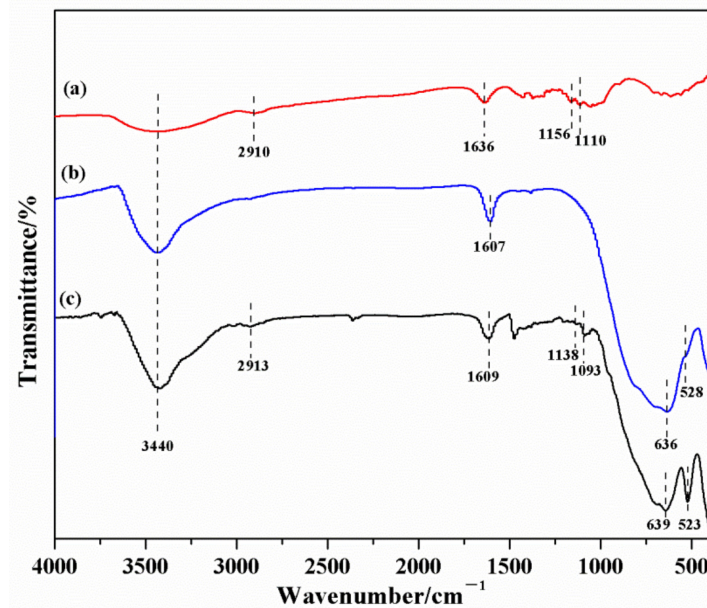


Figure 9. FTIR spectra: (a) cotton fabric, (b) Cl/W-1-2, and (c) Cl/W-0.3 cotton fabric.

### 3.9. SEM and EDS Analyses

The SEM images and EDS of cotton fabrics are presented in Figure 10. As shown in Figure 10a,c, the cotton fabric had a smooth surface before modification. After being treated with cationized  $\text{BiOCl}/\text{Bi}_2\text{WO}_6$ , Cl/W-0.3 cotton fabric showed a rough appearance due to the loading of numerous nanoparticles on its surface. As shown in Figure 10e, the EDS images confirmed the presence of Cl, W, Bi, C, and O on the Cl/W-0.3 cotton fabric. The weight fractions of Cl, W, and Bi were about 0.61%, 47.12% and 6.85%, respectively. Therefore, the SEM images and EDS confirmed the loading of the  $\text{BiOCl}/\text{Bi}_2\text{WO}_6$  photocatalyst on cotton fabric.

### 3.10. Ultraviolet Resistance Evaluation

The ultraviolet resistance property of all the fabrics is recorded in Table 1. The cotton fabric had higher UVA and UVB levels than the finished cotton fabrics. The UPF (ultraviolet protection factor) of cotton fabric was only 5.95, which demonstrated poor ultraviolet resistance compared with the finished cotton fabrics. After modification with  $\text{BiOCl}/\text{Bi}_2\text{WO}_6$  photocatalyst, the UVA and UVB of cotton fabrics obviously decreased, while the UPF significantly increased. In particular, Cl/W-0.3 cotton fabric exhibited the optimal ultraviolet resistance performance, with UPF reaching 40.15.

Table 1. Ultraviolet resistance evaluation.

Sample	UVA (%)	UVB (%)	UPF
Cotton fabric	20	15.45	5.95
Cl/W-0.1 cotton fabric	8.36	2.63	31.92
Cl/W-0.2 cotton fabric	5.77	3.10	37.96
Cl/W-0.3 cotton fabric	3.51	3.45	40.15

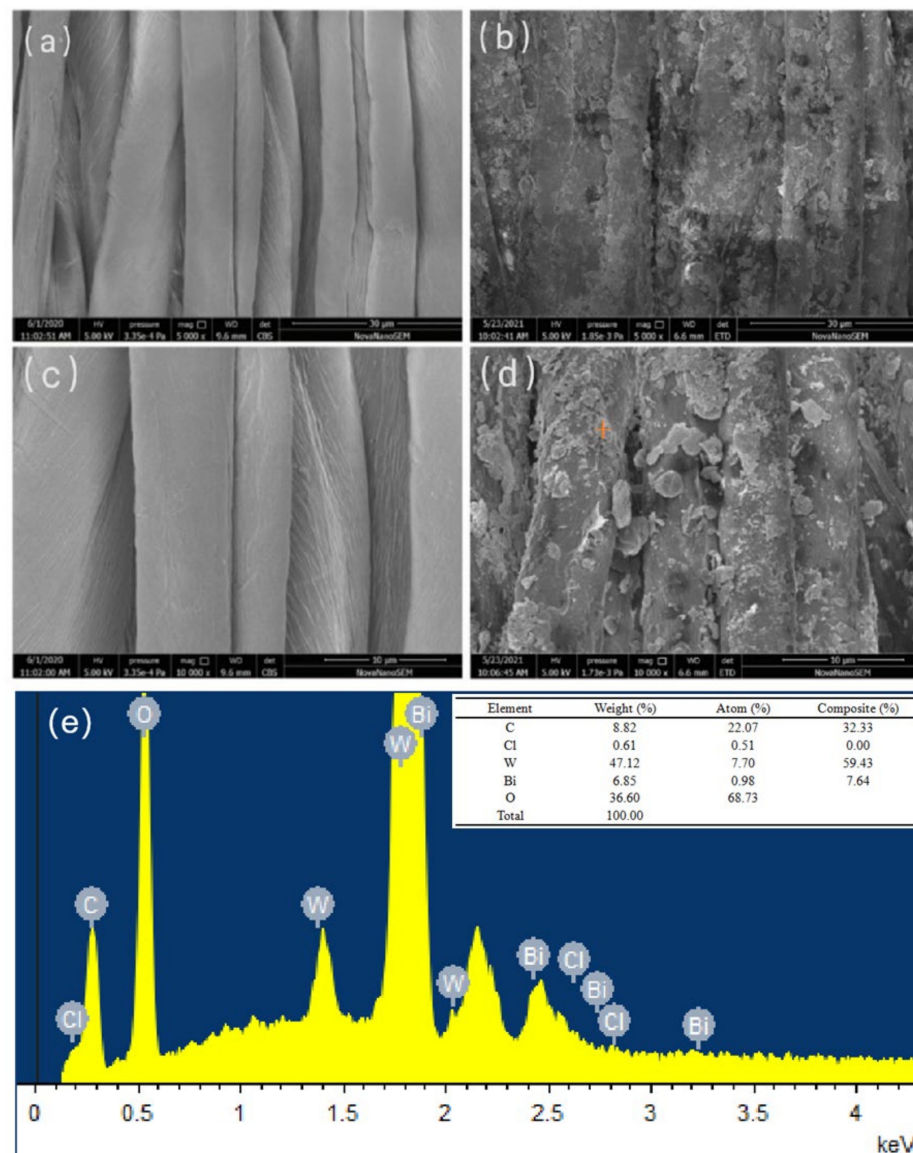


**Figure 10.** SEM images and EDS of cotton fabrics: (a) cotton fabric ( $\times 5000$ ), (b) Cl/W-0.3 cotton fabric ( $\times 5000$ ), (c) cotton fabric ( $\times 10,000$ ), (d) Cl/W-0.3 cotton fabric ( $\times 10,000$ ), and (e) EDS of Cl/W-0.3 cotton fabric.

### 3.11. Photocatalytic Activity of the Cotton Fabrics

As shown in Figure 11a, with the extension of irradiation time, the photodegradation efficiency of cotton fabric to RhB was basically unchanged, while Cl/W-0.3 cotton fabric had a high photodegradation rate of 97.06%. Therefore, the finished cotton fabric had remarkable photocatalytic performance. As shown in Figure 11b, the pseudo-first-order kinetic constant of the Cl/W-0.3 cotton fabric was about  $368.9 \times 10^{-4} \text{ min}^{-1}$ , which was about 51.76 times that of cotton fabric ( $7.12702 \times 10^{-4} \text{ min}^{-1}$ ). Hence, the finishing of BiOCl/Bi<sub>2</sub>WO<sub>6</sub> onto the cotton fabric increased the photocatalytic rate.

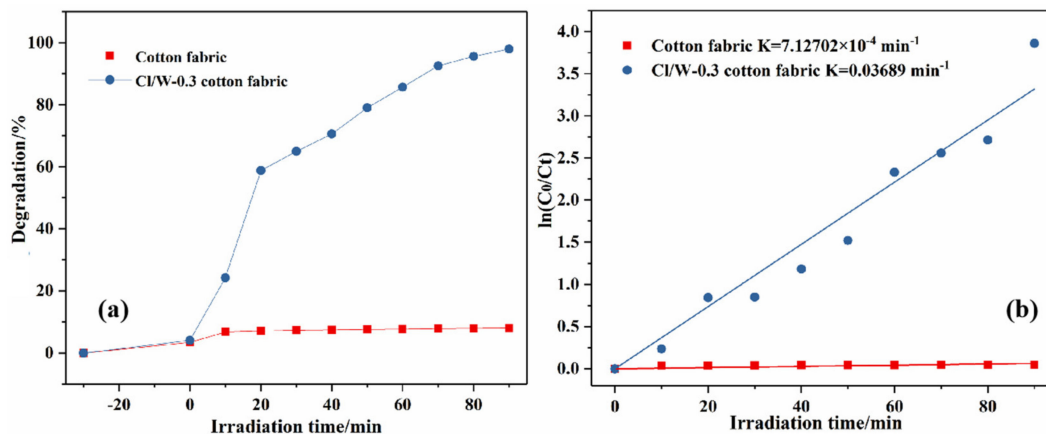


**Figure 11.** Photocatalytic degradation for RhB by cotton fabrics: (a) photodegradation curves and (b) pseudo-first-order kinetic curves.

### 3.12. Self-Cleaning Evaluation

Figure 12 shows the self-cleaning effects of cotton fabric and Cl/W-0.3 cotton fabric to organic pollutants under simulated visible-light irradiation. Cotton fabric faded indistinctly after irradiation for 120 min. For Cl/W-0.3 cotton fabric, after 40 min of exposure to visible light, the red wine and MB solution showed slight decoloration. After 120 min of irradiation, the solutions stained with red wine and MB were both obviously discolored, indicating that the finished cotton fabric with BiOCl/Bi<sub>2</sub>WO<sub>6</sub> had far better self-cleaning performance than cotton fabric [43].

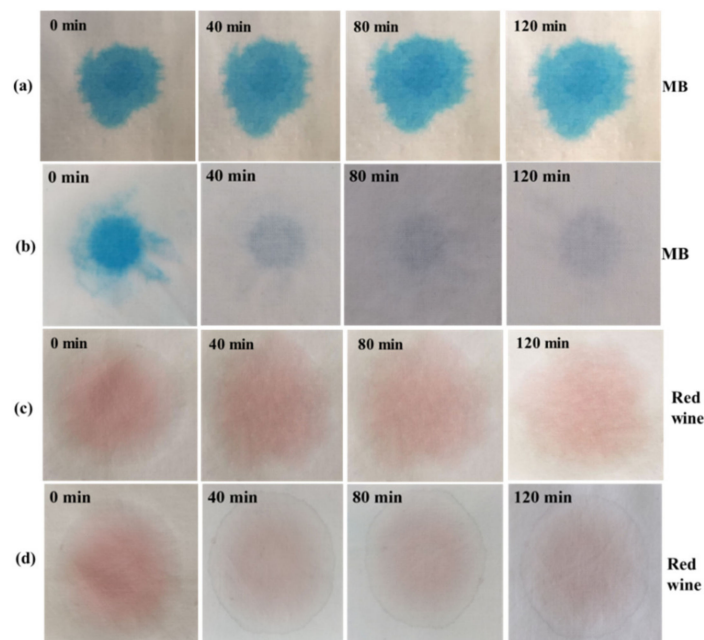


**Figure 12.** Self-cleaning effects of (a,c) cotton fabric, and (b,d) Cl/W-0.3 cotton fabric.

## 4. Conclusions

A nanoflower-shaped BiOCl/Bi<sub>2</sub>WO<sub>6</sub> photocatalyst was synthesized through a simple and efficient hydrothermal method. When the molar ratio of Cl to W was 1:2, the prepared BiOCl/Bi<sub>2</sub>WO<sub>6</sub> exhibited higher photocatalytic activities than the bare BiOCl, Bi<sub>2</sub>WO<sub>6</sub>, and other BiOCl/Bi<sub>2</sub>WO<sub>6</sub> composites under simulated visible-light illumination. Cotton fabric was carboxymethylated with NaOH and sodium chloroacetate solution and further finished with cationized BiOCl/Bi<sub>2</sub>WO<sub>6</sub> to achieve the finished cotton fabric. The experimental results showed that the cotton fabric finished with the BiOCl/Bi<sub>2</sub>WO<sub>6</sub> photocatalyst exhibited commendable UV shielding, photocatalytic, and self-cleaning properties. Hence,

the BiOCl/Bi<sub>2</sub>WO<sub>6</sub>-finished cotton fabrics have broad application prospects in the textile, environmental purification, and medical industries.

**Author Contributions:** Conceptualization, J.C. and K.W.; methodology, J.C. and K.W.; software, Jiayi Chen and K.W.; validation, Z.Q. and C.W.; formal analysis, J.C. and K.W.; investigation, J.T.; resources, N.L.; data curation, W.Y. and Y.C.; writing—original draft preparation, J.C. and N.L.; writing—review and editing, J.C. and C.W.; supervision, C.W. All authors have read and agreed to the published version of the manuscript.

**Funding:** This research received no external funding.

**Institutional Review Board Statement:** Not applicable.

**Informed Consent Statement:** Not applicable.

**Data Availability Statement:** Not applicable.

**Conflicts of Interest:** The authors declare no conflict of interest.

## References

1. Ye, M.; Chen, Z.; Wang, W.; Ma, J.; Shen, J. Hydrothermal synthesis of TiO<sub>2</sub> hollow microspheres for the photocatalytic degradation of 4-chloronitrobenzene. *J. Hazard. Mater.* **2010**, *184*, 612–619. [[CrossRef](#)]
2. Rueda-Marquez, J.J.; Levchuk, I.; Ibañez, P.F.; Sillanpää, M. A critical review on application of photocatalysis for toxicity reduction of real wastewaters. *J. Clean. Prod.* **2020**, *258*, 120694. [[CrossRef](#)]
3. Iervolino, G.; Zammit, I.; Vaiano, V.; Rizzo, L. Limitations and Prospects for Wastewater Treatment by UV and Visible-Light-Active Heterogeneous Photocatalysis: A Critical Review. *Top. Curr. Chem.* **2020**, *378*, 7. [[CrossRef](#)]
4. Liu, W.; He, T.; Wang, Y.; Ning, G.; Xu, Z.; Chen, X.; Hu, X.; Wu, Y.; Zhao, Y. Synergistic adsorption-photocatalytic degradation effect and norfloxacin mechanism of ZnO/ZnS@BC under UV-light irradiation. *Sci. Rep.* **2020**, *10*, 11903. [[CrossRef](#)]
5. Ivetić, T.B.; Finčur, N.L.; Abramović, B.F.; Dimitrievska, M.; Štrbac, G.R.; Čajko, K.O.; Miljević, B.B.; Đaćanin, L.R.; Lukić-Petrović, S.R. Environmentally friendly photoactive heterojunction zinc tin oxide nanoparticles. *Ceram. Int.* **2016**, *42*, 3575–3583. [[CrossRef](#)]
6. Jeon, J.; Kweon, D.H.; Jang, B.J.; Ju, M.J.; Baek, J. Enhancing the Photocatalytic Activity of TiO<sub>2</sub> Catalysts. *Adv. Sustain. Syst.* **2020**, *4*, 2000197. [[CrossRef](#)]
7. Gu, X.; Li, C.; Yuan, S.; Ma, M.; Qiang, Y.; Zhu, J. ZnO based heterojunctions and their application in environmental photocatalysis. *Nanotechnology* **2016**, *27*, 402001. [[CrossRef](#)] [[PubMed](#)]
8. Yao, L.; Yang, H.; Chen, Z.; Qiu, M.; Hu, B.; Wang, X. Bismuth oxychloride-based materials for the removal of organic pollutants in wastewater. *Chemosphere* **2021**, *273*, 128576. [[CrossRef](#)]
9. Fazal, T.; Razaq, A.; Javed, F.; Hafeez, A.; Rashid, N.; Amjad, U.S.; Rehman, M.S.U.; Faisal, A.; Rehman, F. Integrating adsorption and photocatalysis: A cost effective strategy for textile wastewater treatment using hybrid biochar-TiO<sub>2</sub> composite. *J. Hazard. Mater.* **2020**, *390*, 121623. [[CrossRef](#)] [[PubMed](#)]
10. Chang, J.; Zhong, Y.; Hu, C.; Luo, J.; Wang, P. Hollow microspheres of BiOCl assembled with nanosheets: Spray drying synthesis and drastically enhanced photocatalytic activity. *J. Environ. Chem. Eng.* **2018**, *6*, 6971–6978. [[CrossRef](#)]
11. Chang, X.; Gondal, M.A.; Al-Saadi, A.A.; Ali, M.A.; Shen, H.; Zhou, Q.; Zhang, J.; Du, M.; Liu, Y.; Ji, G. Photodegradation of Rhodamine B over unexcited semiconductor compounds of BiOCl and BiOBr. *J. Colloid Interf. Sci.* **2012**, *377*, 291–298. [[CrossRef](#)] [[PubMed](#)]
12. Gao, X.; Fei, J.; Dai, Y.; Fu, F. Hydrothermal synthesis of series Cu-doped Bi<sub>2</sub>WO<sub>6</sub> and its application in photo-degradative removal of phenol in wastewater with enhanced efficiency. *J. Mol. Liq.* **2018**, *256*, 267–276. [[CrossRef](#)]
13. An, W.; Wang, S.; Fu, Y.; Guan, Y.; Li, Z.; Xu, T.; Wang, H. Construction of Bi<sub>2</sub>WO<sub>6</sub> with oxygen vacancies and investigation on mechanisms of significantly enhanced photocatalytic activity. *Desalin. Water Treat.* **2021**, *216*, 151–161. [[CrossRef](#)]
14. Guo, M.; Zhou, Z.; Yan, S.; Zhou, P.; Miao, F.; Liang, S.; Wang, J.; Cui, X. Bi<sub>2</sub>WO<sub>6</sub>-BiOCl heterostructure with enhanced photocatalytic activity for efficient degradation of oxytetracycline. *Sci. Rep.* **2020**, *10*, 18401. [[CrossRef](#)] [[PubMed](#)]
15. Yang, K.; Li, X.; Yu, C.; Zeng, D.; Chen, F.; Zhang, K.; Huang, W.; Ji, H. Review on heterophase/homophase junctions for efficient photocatalysis: The case of phase transition construction. *Chin. J. Catal.* **2019**, *40*, 796–818. [[CrossRef](#)]
16. Ivetic, T.B.; Fincur, N.L.; Merkulov, D.V.S.; Despotovic, V.N.; Cetojevic-Simin, D.D.; Armakovic, S.J.; Uzelac, M.M.; Bognár, S.I.; Zec, N.J.; Lukic-Petrovic, S.R.; et al. Water-Active Titanium/Molybdenum/Mixed-Oxides: Removal Efficiency of Organic Water Pollutants by Adsorption and Photocatalysis and Toxicity Assessment. *Catalysts* **2021**, *11*, 1054. [[CrossRef](#)]
17. Tahmasebi, N.; Maleki, Z.; Farahnak, P. Enhanced photocatalytic activities of Bi<sub>2</sub>WO<sub>6</sub>/BiOCl composite synthesized by one-step hydrothermal method with the assistance of HCl. *Mat. Sci. Semicon. Proc.* **2019**, *89*, 32–40. [[CrossRef](#)]
18. Liang, Z.; Zhou, C.; Yang, J.; Mo, Q.; Zhang, Y.; Tang, Y. Visible light responsive Bi<sub>2</sub>WO<sub>6</sub>/BiOCl heterojunction with enhanced photocatalytic activity for degradation of tetracycline and rohdamine B. *Inorg. Chem. Commun.* **2018**, *93*, 136–139. [[CrossRef](#)]

19. Pal, S.; Mondal, S.; Maity, J. Synthesis, characterization and photocatalytic properties of ZnO nanoparticles and cotton fabric modified with ZnO nanoparticles via in-situ hydrothermal coating technique: Dual response. *Mater. Technol.* **2018**, *33*, 884–891. [[CrossRef](#)]
20. Wang, C.; Lv, J.; Ren, Y.; Zhou, Q.; Chen, J.; Zhi, T.; Lu, Z.; Gao, D.; Ma, Z.; Jin, L. Cotton fabric with plasma pretreatment and ZnO/Carboxymethyl chitosan composite finishing for durable UV resistance and antibacterial property. *Carbohydr. Polym.* **2016**, *138*, 106–113.
21. Yang, M.; Liu, W.; Jiang, C.; Xie, Y.; Shi, H.; Zhang, F.; Wang, Z. Facile construction of robust superhydrophobic cotton textiles for effective UV protection, self-cleaning and oil-water separation. *Colloid. Surf. A* **2019**, *570*, 172–181. [[CrossRef](#)]
22. Hu, J.; Gao, Q.; Xu, L.; Wang, M.; Zhang, M.; Zhang, K.; Liu, W.; Wu, G. Functionalization of cotton fabrics with highly durable polysiloxane–TiO<sub>2</sub> hybrid layers: Potential applications for photo-induced water–oil separation, UV shielding, and self-cleaning. *J. Mater. Chem. A* **2018**, *6*, 6085–6095. [[CrossRef](#)]
23. Wang, Y.; Ding, X.; Zhang, P.; Wang, Q.; Zheng, K.; Chen, L.; Ding, J.; Tian, X.; Zhang, X. Convenient and recyclable TiO<sub>2</sub>/g-C<sub>3</sub>N<sub>4</sub> photocatalytic coating: Layer-by-layer self-assembly construction on cotton fabrics leading to improved catalytic activity under visible light. *Ind. Eng. Chem. Res.* **2019**, *58*, 3978–3987. [[CrossRef](#)]
24. Cao, C.; Wang, F.; Lu, M. Superhydrophobic CuO coating fabricated on cotton fabric for oil/water separation and photocatalytic degradation. *Colloid. Surf. A* **2020**, *601*, 125033. [[CrossRef](#)]
25. Wang, K.; Song, X.; Li, Y.; Tian, J.; Zhang, C.; Qi, Z.; Liu, S.; Gao, D.; Liu, G.; Ren, Y.; et al. In Situ Precipitation of Ag<sub>6</sub>Si<sub>2</sub>O<sub>7</sub> on the Surface of Cotton Fabric Modified by Plasma Treatment for Highly Efficient and Durable Photocatalytic Activity. *Integr. Ferroelectr.* **2021**, *219*, 111–118. [[CrossRef](#)]
26. Tudu, B.K.; Sinhamahapatra, A.; Kumar, A. Surface modification of cotton fabric using TiO<sub>2</sub> nanoparticles for self-cleaning, oil-water separation, antistain, anti-water absorption, and antibacterial properties. *ACS Omega* **2020**, *5*, 7850–7860. [[CrossRef](#)]
27. Jin, J.; Feng, K.; Liu, X. Enhanced photocatalytic degradation and UV protection properties of BiOCl nanosheets coating for cotton fabric. *Funct. Mater. Lett.* **2018**, *11*, 1850052. [[CrossRef](#)]
28. Wu, J.; Zhang, W.; Tian, Z.; Zhao, Y.; Shen, Z. Facile fabrication of Bi<sub>2</sub>WO<sub>6</sub>/BiOCl hierarchical structure as adsorbents for methylene blue dye removal. *Mater. Res. Express* **2019**, *6*, 055034. [[CrossRef](#)]
29. Qi, Z.; Wang, K.; Jiang, Y.; Zhu, Y.; Chen, X.; Tang, Q.; Ren, Y.; Zheng, C.; Gao, D.; Wang, C. Preparation and characterization of SnO<sub>2</sub>-x/GO composite photocatalyst and its visible light photocatalytic activity for self-cleaning cotton fabrics. *Cellulose* **2019**, *26*, 8919–8937. [[CrossRef](#)]
30. Liu, Y.; Xia, L.; Guo, H.; Wang, A.; Hu, J.; Zhang, W.; Xu, W.; Wang, Y. Kinetics and thermodynamics studies of cationic dye adsorption onto carboxymethyl cotton fabric. *J. Nat. Fibers* **2020**, 1–12. [[CrossRef](#)]
31. Wang, C.; Xu, L.; Wang, K.; Chen, H.; Jiang, W.; Qi, Z.; Gao, D.; Liu, S.; Song, X.; Liu, G.; et al. Ag<sub>6</sub>Si<sub>2</sub>O<sub>7</sub>/CNTs with highly efficient and stable visible light photocatalytic activity. *Integr. Ferroelectr.* **2019**, *198*, 73–79. [[CrossRef](#)]
32. Wang, K.; Zhuo, Y.; Chen, J.; Gao, D.; Ren, Y.; Wang, C.; Qi, Z. Crystalline phase regulation of anatase–rutile TiO<sub>2</sub> for the enhancement of photocatalytic activity. *RSC Adv.* **2020**, *10*, 43592–43598. [[CrossRef](#)]
33. Gao, D.; Wang, L.; Wang, C.; Chen, T. Photocatalytic self-cleaning cotton fabrics coated by Cu<sub>2</sub>(OH)PO<sub>4</sub> under Vis/NIR irradiation. *Materials* **2019**, *12*, 238. [[CrossRef](#)]
34. Zhao, Y.; Chen, T.; Ma, R.; Du, J.; Xie, C. Synthesis of flower-like CeO<sub>2</sub>/BiOCl heterostructures with enhanced ultraviolet light photocatalytic activity. *Micro. Nano Lett.* **2018**, *13*, 1394–1398. [[CrossRef](#)]
35. Zhou, Y.; Lv, P.; Zhang, W.; Meng, X.; He, H.; Zeng, X.; Shen, X. Pristine Bi<sub>2</sub>WO<sub>6</sub> and hybrid Au-Bi<sub>2</sub>WO<sub>6</sub> hollow microspheres with excellent photocatalytic activities. *Appl. Surf. Sci.* **2018**, *457*, 925–932. [[CrossRef](#)]
36. Hojamberdiev, M.; Kadirova, Z.C.; Zahedi, E.; Onna, D.; Marchi, M.C.; Zhu, G.; Matsushita, N.; Hasegawa, M.; Bilmes, S.A.; Okada, K. Tuning the morphological structure, light absorption, and photocatalytic activity of Bi<sub>2</sub>WO<sub>6</sub> and Bi<sub>2</sub>WO<sub>6</sub>-BiOCl through cerium doping. *Arab. J. Chem.* **2020**, *13*, 2844–2857. [[CrossRef](#)]
37. Dumrongrojthanath, P.; Saksoong, T.; Patiphatpanya, P.; Phuruangrat, A.; Thongtem, S.; Thongtem, T. Microwave-assisted hydrothermal synthesis of BiOCl/Bi<sub>2</sub>WO<sub>6</sub> nanocomposites for the enhancement of photocatalytic efficiency. *Res. Chem. Intermed.* **2019**, *45*, 2301–2312. [[CrossRef](#)]
38. Ma, Y.; Chen, Z.; Qu, D.; Shi, J. Synthesis of chemically bonded BiOCl@Bi<sub>2</sub>WO<sub>6</sub> microspheres with exposed (0 2 0) Bi<sub>2</sub>WO<sub>6</sub> facets and their enhanced photocatalytic activities under visible light irradiation. *Appl. Surf. Sci.* **2016**, *361*, 63–71. [[CrossRef](#)]
39. Zhu, S.; Yang, C.; Li, F.; Li, T.; Zhang, M.; Cao, W. Improved photocatalytic Bi<sub>2</sub>WO<sub>6</sub>/BiOCl heterojunctions: One-step synthesis via an ionic-liquid assisted ultrasonic method and first-principles calculations. *Mol. Catal.* **2017**, *435*, 33–48. [[CrossRef](#)]
40. Qi, Z.; Wang, K.; Chen, J.; Gao, D.; Ren, Y.; Wang, C. Cotton fabric loaded with self-dispersive and reactive biphasic TiO<sub>2</sub> for durable self-cleaning activity and ultraviolet protection. *New J. Chem.* **2021**, *45*, 11119–11129. [[CrossRef](#)]
41. Wang, J.; Wei, Y.; Yang, B.; Wang, B.; Chen, J.; Jing, H. In situ grown heterojunction of Bi<sub>2</sub>WO<sub>6</sub>/BiOCl for efficient photoelectrocatalytic CO<sub>2</sub> reduction. *J. Catal.* **2019**, *377*, 209–217. [[CrossRef](#)]
42. Thi, V.H.T.; Lee, B.-K.J. Development of multifunctional self-cleaning and UV blocking cotton fabric with modification of photoactive ZnO coating via microwave method. *Photoch. Photobiol. A* **2017**, *338*, 13–22.
43. Zheng, C.; Qi, Z.; Shen, W.; Chen, G. Self-cleaning Bombyx mori silk: Room-temperature preparation of anatase nano-TiO<sub>2</sub> by the sol-gel method and its application. *Color. Technol.* **2014**, *130*, 280–287. [[CrossRef](#)]